

469 **Boarder Impact**

470 Mirror Diffusion Models (MDMs) advance the recent development of diffusion models to complex
 471 domains subjected to convex constrained sets. This opens up new possibilities for MDMs to serve as
 472 preferred models for generating samples that live in *e.g.*, simplices and balls. Additionally, MDMs
 473 introduce an innovative application of constrained sets as a watermarking technique. This has the
 474 potential to address concerns related to unethical usage and safeguard the copyright of generative
 475 models. By incorporating constrained sets into the generating process, MDMs offer a means to
 476 prevent unauthorized usage and ensure the integrity of generated content.

477 **A Derivation of Mirror Mappings**

478 Here, we provide addition derivation of $\nabla\phi^*$. Computation of $\nabla\phi(x)$ and $\nabla^2\phi^*(y)$ follow straight-
 479 forwardly by differentiating $\phi(x)$ and $\nabla\phi^*(y)$ w.r.t. x and y , respectively.

480 **ℓ_2 -Ball** Since the gradient map also reverses the mirror map, we aim to rewrite $y = \frac{2\gamma}{R - \|x\|_2^2}x$ as
 481 $x = f(y) = \nabla\phi_{\text{ball}}^*(y)$. Solving the second-order polynomial,

$$\|y\|_2^2 = \left(\frac{2\gamma}{R - \|x\|_2^2} \right)^2 \|x\|_2^2, \quad (19)$$

482 yields

$$\|x\|_2^2 = R + \frac{2\gamma}{\|y\|_2^2} \left(\gamma - \sqrt{R\|y\|_2^2 + \gamma^2} \right). \quad (20)$$

483 With that, we can rewrite Equation (11) by

$$x = \frac{R - \|x\|_2^2}{2\gamma} y \stackrel{(20)}{=} \frac{\sqrt{R\|y\|_2^2 + \gamma^2} - \gamma}{\|y\|_2^2} y = \frac{R}{\sqrt{R\|y\|_2^2 + \gamma^2} + \gamma} y.$$

484 **Simplex** Standard calculations in convex analysis [28] shows

$$\phi_{\text{simplex}}^*(y) = \log \left(1 + \sum_i^d e^{y_i} \right). \quad (21)$$

485 Differentiating Equation (21) w.r.t. y yields $\nabla\phi_{\text{simplex}}^*$ in Equation (13).

486 **Polytope** Since the gradient map also reverses the mirror map, we aim to inverse

$$y = \sum_{i=1}^m s_i \langle a_i, x \rangle a_i + \sum_{j=m+1}^d \langle a_j, x \rangle a_j. \quad (22)$$

487 When all d constraints are orthonormal, taking inner product between y and each a yields

$$\langle a_i, y \rangle = s_i \langle a_i, x \rangle, \quad \langle a_j, y \rangle = \langle a_j, x \rangle. \quad (23)$$

488 Therefore, we can reconstruct x from y via

$$\begin{aligned} x &= \sum_{i=1}^m \langle a_i, x \rangle a_i + \sum_{j=m+1}^d \langle a_j, x \rangle a_j \\ &\stackrel{(23)}{=} \sum_{i=1}^m s_i^{-1} \langle a_i, y \rangle a_i + \sum_{j=m+1}^d \langle a_j, y \rangle a_j, \end{aligned}$$

489 which defines $x = \nabla\phi_{\text{polytope}}^*(y)$. For completeness, the Hessian can be presented compactly as

$$\nabla^2\phi_{\text{polytope}}^*(y) = \mathbf{I} + \mathbf{A}\Sigma\mathbf{A}^\top, \quad (24)$$

490 where \mathbf{I} is the identity matrix, $\mathbf{A} := [a_1, \dots, a_m]$ is a d -by- m matrix whose column vector a_i
 491 corresponds to each constraint, and $\Sigma \in \mathbb{R}^{m \times m}$ is a diagonal matrix with leading entries

$$[\Sigma]_{ii} = \frac{\partial s_i^{-1}(z)}{\partial z} \Big|_{z=\langle a_i, y \rangle} - 1 \stackrel{(18)}{=} \frac{b_i - c_i}{2} (1 - \tanh^2(\langle a_i, y \rangle)) - 1.$$

492 **B Additional Remarks on Polytope**

493 **Derivation of Equation (17)** Since the subspaces spanned by $\{a_i\}$ and $\{a_j\}$ are orthogonal to each
 494 other, we can rewrite (15) as

$$\nabla\phi_{\text{polytope}}(x) = \sum_{i=1}^m s_i(\langle a_i, x \rangle) a_i + \left(x - \sum_{i=1}^m \langle a_i, x \rangle a_i \right) = x + \sum_{i=1}^m (s_i(\langle a_i, x \rangle) - \langle a_i, x \rangle) a_i.$$

495 $\nabla\phi_{\text{polytope}}^*(y)$ follows similar derivation.

496 **Generalization to non-orthonormal constraints** The mirror maps of a polytope, as described in
 497 Equations (15) to (17), can be seen as operations that manipulate the coefficients associated with
 498 the bases defined by the constraints. This understanding allows us to extend the computation to
 499 non-orthonormal constraints by identifying the corresponding ‘‘coefficients’’ through a change of
 500 bases, utilizing the reproducing formula:

$$x = \sum_{i=1}^d \langle \tilde{a}_i, x \rangle a_i, \text{ where } \tilde{a}_i \text{ is the } i\text{-th row of } (\mathbf{A}^\top \mathbf{A})^{-1} \mathbf{A}^\top,$$

501 and $\mathbf{A} := [a_1, \dots, a_m]$. Similarly, we have $y = \sum_{i=1}^d \langle \tilde{a}_i, y \rangle a_i$. Applying similar derivation leads to

$$\nabla\phi_{\text{poly}}(x) = x + \sum_{i=1}^m (s_i(\langle \tilde{a}_i, x \rangle) - \langle \tilde{a}_i, x \rangle) a_i, \quad \nabla\phi_{\text{poly}}^*(y) = y + \sum_{i=1}^m (s_i^{-1}(\langle \tilde{a}_i, y \rangle) - \langle \tilde{a}_i, y \rangle) a_i.$$

502 **C Experiment Details & Additional Results**

Table 7: The concentration parameter α of each Dirichlet distribution in simplices constrained sets.

d	3	3	7	9	20
α	[2, 4, 8]	[1, 0.1, 5]	[1, 2, 2, 4, 4, 8, 8]	[1, 0.5, 2, 0.3, 0.6, 4, 8, 8, 2]	[0.2, 0.4, \dots , 4, 4.2]

Table 8: Hyperparameters of the polytope $\mathcal{M} := \{x \in \mathbb{R}^d : c_i < a_i^\top x < b_i\}$ for each dataset and watermark precision. Note that we fix $b = b_i = -c_i$ in practice.

<i>Precision</i>	FFHQ 64×64 (uncon)			AFHQv2 64×64 (uncon)		
	59.3%	71.8%	93.3%	56.9%	75.0%	92.7%
Number of constraints m	7	20	100	4	20	100
Constraint range b	1.05	1.05	1.05	0.9	0.9	0.9

503 **Dataset & constrained sets**

- 504 • *ℓ_2 -balls constrained sets*: For $d = 2$, we consider the Gaussian Mixture Model (with variance
 505 0.05) and the Spiral shown respectively in Figures 1 and 3. For $d = \{6, 8, 20\}$, we place d
 506 isotropic Gaussians, each with variance 0.05, at the corner of each dimension, and reject samples
 507 outside the constrained sets.
- 508 • *Simplices constrained sets*: We consider Dirichlet distributions [48], $\text{Dir}(\alpha)$, with various con-
 509 centration parameters α detailed in Table 7.
- 510 • *Hypercube constrained sets*: For all dimensions $d = \{2, 3, 6, 8, 20\}$, we place d isotropic
 511 Gaussians, each with variance 0.2, at the corner of each dimension, and either reject ($d =$
 512 $\{2, 3, 6, 8\}$) or reflect ($d = 20$) samples outside the constrained sets.
- 513 • *Watermarked datasets and polytope constrained sets*: We follow the same data preprocessing from
 514 EDM³ [38] and rescale both FFHQ and AFHQv2 to 64×64 image resolution. For the polytope
 515 constrained sets $\mathcal{M} := \{x \in \mathbb{R}^d : c_i < a_i^\top x < b_i, \forall i\}$, we construct a_i from orthonormalized
 516 Gaussian random vectors and detail other hyperparameters in Table 8.

³<https://github.com/NVlabs/edm>, released under Nvidia Source Code License.

517 **Implementation** All methods are implemented in PyTorch [72]. We adopt ADM⁴ and EDM³ [38]
 518 respectively as the MDM’s diffusion backbones for constrained and watermarked generation. We
 519 implemented Reflected Diffusion [18] by ourselves as their codes have not yet been made available,
 520 and used the official implementation⁵ of Reflected Diffusion [25] in Table 11. We also implemented
 521 Simplex Diffusion [60], but as observed in previous works [25], it encountered computational
 522 instability especially when computing the modified Bessel functions.

523 **Training** For constrained generation, all methods are trained with AdamW [73] and an exponential
 524 moving average with the decay rate of 0.99. As standard practices, we decay the learning rate by the
 525 decay rate 0.99 every 1000 steps. For watermarked generation, we follow the default hyperparameters
 526 from EDM³ [38]. All experiments are conducted on two TITAN RTXs and one RTX 2080.

527 **Network** For constrained generation, all networks take (y, t) as inputs and follow

$$\text{out} = \text{out_mod}(\text{norm}(y_mod(y) + t_mod(\text{timestep_embedding}(t))))),$$

528 where $\text{timestep_embedding}(\cdot)$ is the standard sinusoidal embedding. t_mod and out_mod consist
 529 of 2 fully-connected layers (Linear) activated by the Sigmoid Linear Unit (SiLU) [74]:

$$t_mod = out_mod = \text{Linear} \rightarrow \text{SiLU} \rightarrow \text{Linear}$$

530 and y_mod consists of 3 residual blocks, *i.e.*, $y_mod(y) = y + \text{res_mod}(\text{norm}(y))$, where

$$\text{res_mod} = \text{Linear} \rightarrow \text{SiLU} \rightarrow \text{Linear} \rightarrow \text{SiLU} \rightarrow \text{Linear} \rightarrow \text{SiLU} \rightarrow \text{Linear}$$

531 All Linear’s have 128 hidden dimension. We use group normalization [75] for all norm. For
 532 watermarked generation, we use EDM parameterization³ [38].

533 **Evaluation** We compute the Wasserstein and Sliced Wasserstein distances using the `geomloss`⁶
 534 and `ot`⁷ packages, respectively. The Maximum Mean Discrepancy (MMD) is based on the popular
 535 package https://github.com/ZongxianLee/MMD_Loss.Pytorch, which is unlicensed. For
 536 watermarked generation, we follow the same evaluation pipeline from EDM³ [38] by first generating
 537 50,000 watermarked samples and computing the FID w.r.t. the training statistics.

538 C.1 Additional Results

539 **Tractable variational bound in Equation (8)** Figure 9 demon-
 540 strates how MDM faithfully captures the variational bound to the
 541 negative log-likelihood (NLL) of 2-dimensional GMM.

542 **More constrained sets, distributional metrics, & baseline** Tables 9 and 10 expand the analysis in Tables 3 and 4 with additional
 543 distributional metrics such as Wasserstein-1 (\mathcal{W}_1) and Maximum
 544 Mean Discrepancy (MMD). Additionally, Table 11 reports the
 545 results of hypercube $[0, 1]^d$ constrained set, a special instance
 546 of polytopes, and includes additional baseline from Lou and Ermon [25], which approximate the
 547 intractable scores in Reflected Diffusion using eigenfunctions tailored specifically to hypercubes,
 548 rather than implicit score matching as in Fishman et al. [18]. Consistently, our findings conclude
 549 that the MDM is the *only* constrained-based diffusion model that achieves comparable or better
 550 performance to DDPM. These results affirm the effectiveness of MDM in generating high-quality
 551 samples within constrained settings, making it a reliable choice for constrained generative modeling.
 552

553 **More watermarked samples** Figures 10 and 11 provide additional qualitative results on the
 554 watermarked samples generated by MDMs.

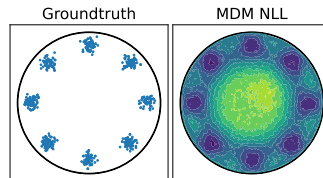


Figure 9: Tractable variational bound by our MDM.

⁴<https://github.com/openai/guided-diffusion>, released under MIT License.

⁵<https://github.com/louaaron/Reflected-Diffusion>, latest commit (65d05c6) at submission, unlicensed.

⁶<https://github.com/jeanfeydy/geomloss>, released under MIT License.

⁷https://pythonot.github.io/gen_modules/ot.sliced.html#ot.sliced.sliced_wasserstein_distance, released under MIT License.

Table 9: Expanded results of ℓ_2 -ball constrained sets, where we include additional distributional metrics such as \mathcal{W}_1 and Maximum Mean Discrepancy (MMD), all computed with 1000 samples and averaged over three trials. Consistently, our findings conclude that the MDM is the *only* constrained-based diffusion model that achieves comparable or better performance to DDPM.

	$d = 2$	$d = 2$	$d = 6$	$d = 8$	$d=20$
$\mathcal{W}_1 \downarrow$ (unit: 10^{-2})					
DDPM [2]	0.66 ± 0.15	0.14 ± 0.03	0.52 ± 0.09	0.58 ± 0.10	3.45 ± 0.50
Reflected [18]	0.55 ± 0.29	0.46 ± 0.17	3.11 ± 0.40	10.13 ± 0.21	19.42 ± 0.13
MDM (ours)	0.46 ± 0.07	0.12 ± 0.04	0.72 ± 0.39	1.05 ± 0.26	2.63 ± 0.31
$\text{MMD} \downarrow$ (unit: 10^{-2})					
DDPM [2]	0.67 ± 0.23	0.23 ± 0.07	0.37 ± 0.19	0.75 ± 0.24	0.98 ± 0.42
Reflected [18]	0.58 ± 0.46	5.03 ± 1.17	2.34 ± 0.14	28.82 ± 0.66	14.83 ± 0.62
MDM (ours)	0.52 ± 0.36	0.27 ± 0.19	0.54 ± 0.12	0.35 ± 0.23	0.50 ± 0.17
Constraint violation (%) \downarrow					
DDPM [2]	0.00 ± 0.00	0.00 ± 0.00	8.67 ± 0.87	13.60 ± 0.62	19.33 ± 1.29

Table 10: Expanded results of simplices constrained sets.

	$d = 3$	$d = 3$	$d = 7$	$d = 9$	$d=20$
$\mathcal{W}_1 \downarrow$ (unit: 10^{-2})					
DDPM [2]	0.01 ± 0.00	0.02 ± 0.01	0.03 ± 0.00	0.05 ± 0.00	0.11 ± 0.00
Reflected [18]	0.06 ± 0.01	0.12 ± 0.00	0.62 ± 0.08	3.57 ± 0.05	0.98 ± 0.02
MDM (ours)	0.01 ± 0.00	0.01 ± 0.01	0.03 ± 0.00	0.05 ± 0.00	0.13 ± 0.00
$\text{MMD} \downarrow$ (unit: 10^{-2})					
DDPM [2]	0.72 ± 0.07	0.72 ± 0.30	0.74 ± 0.10	0.97 ± 0.22	1.12 ± 0.07
Reflected [18]	3.91 ± 0.95	15.12 ± 1.36	16.48 ± 1.04	131.44 ± 2.65	57.90 ± 2.07
MDM (ours)	0.44 ± 0.16	0.50 ± 0.26	0.42 ± 0.08	0.55 ± 0.13	0.61 ± 0.03
Constraint violation (%) \downarrow					
DDPM [2]	0.73 ± 0.12	14.40 ± 1.39	11.63 ± 0.90	27.53 ± 0.57	68.83 ± 1.66

Table 11: Results of hypercube $[0, 1]^d$ constrained sets.

	$d = 2$	$d = 3$	$d = 6$	$d = 8$	$d=20$
Sliced Wasserstein \downarrow (unit: 10^{-2})					
DDPM [2]	2.24 ± 1.22	2.17 ± 0.65	2.05 ± 0.41	2.01 ± 0.16	1.54 ± 0.01
Reflected [25]	3.75 ± 1.20	6.58 ± 1.18	2.77 ± 0.06	3.50 ± 0.69	3.37 ± 0.46
Reflected [18]	19.05 ± 1.51	17.16 ± 0.88	11.90 ± 0.43	7.49 ± 0.13	4.32 ± 0.23
MDM (ours)	3.00 ± 0.72	1.92 ± 0.81	1.75 ± 0.17	1.85 ± 0.34	3.35 ± 0.64
$\mathcal{W}_1 \downarrow$ (unit: 10^{-2})					
DDPM [2]	0.07 ± 0.05	0.22 ± 0.07	1.65 ± 0.14	3.30 ± 0.16	16.74 ± 0.12
Reflected [25]	0.20 ± 0.12	1.21 ± 0.39	2.53 ± 0.04	4.82 ± 0.42	25.47 ± 0.20
Reflected [18]	4.40 ± 0.57	6.01 ± 0.97	9.34 ± 0.56	9.84 ± 0.24	25.27 ± 0.36
MDM (ours)	0.08 ± 0.03	0.20 ± 0.07	1.57 ± 0.08	3.34 ± 0.23	20.59 ± 1.19
$\text{MMD} \downarrow$ (unit: 10^{-2})					
DDPM [2]	0.27 ± 0.26	0.32 ± 0.14	0.69 ± 0.21	0.81 ± 0.23	0.73 ± 0.07
Reflected [25]	0.92 ± 0.53	3.56 ± 1.31	1.16 ± 0.04	2.09 ± 0.70	2.83 ± 0.58
Reflected [18]	32.26 ± 3.19	26.64 ± 5.07	29.83 ± 1.42	15.84 ± 0.89	7.21 ± 0.68
MDM (ours)	0.27 ± 0.09	0.29 ± 0.17	0.39 ± 0.14	0.61 ± 0.23	0.62 ± 0.05
Constraint violation (%) \downarrow					
DDPM [2]	9.37 ± 0.12	17.57 ± 1.27	41.70 ± 1.30	59.30 ± 1.39	94.47 ± 0.64

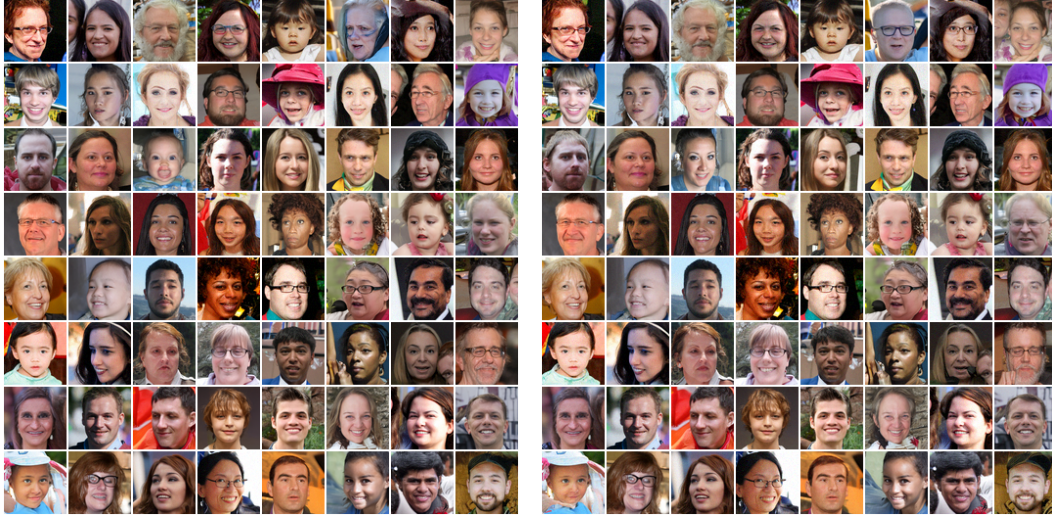


Figure 10: FFHQ 64×64 unconditional watermarked samples generated by **(left)** MDM-proj and **(right)** MDM-dual from the same set of random seeds. Despite the fact that some images, such as the one in the first row and sixth column, were altered possibly due to the change of dual-space distribution (see Figure 7), they look realistic and remain close to the data distribution.



Figure 11: AFHQv2 64×64 unconditional watermarked samples generated by **(left)** MDM-proj and **(right)** MDM-dual from the same set of random seeds. Despite the fact that some images, such as the one in the fifth row and first column, were altered possibly due to the change of dual-space distribution (see Figure 7), they all look realistic and remain close to the data distribution.